

Article

Research on the Ablation Resistance of TiC Particle-Reinforced Aluminium-Based Composite Coatings on Armature Surface

Chenlu Fan ¹, Li Zhang ^{1,*}, Nurbek Nurullougli Kurbonov ² , Ikromjon Usmonovich Rakhmonov ² and Guan Wang ¹

¹ School of Electrical Engineering, Shandong University, Jinan 250061, China; 202214600@mail.sdu.edu.cn (C.F.); guanpallas@sdu.edu.cn (G.W.)

² Power Engineering Faculty, Tashkent State Technical University, Tashkent 100095, Uzbekistan; nurbek.kurbonov.96@gmail.com (N.N.K.); ilider1987@yandex.com (I.U.R.)

* Correspondence: zhleee@sdu.edu.cn

Abstract: The work aims to enhance and modify the armature surface in electromagnetic rail launch systems and improve its anti-ablation performance to better resist the impact ablation effects of high-temperature and high-speed arcs during the electromagnetic rail launch process and improve launch reliability. TiC particles are widely selected as metal material reinforcements, with advantages such as high melting points and high hardness. In this paper, the arc impact model of pure aluminum alloy and the arc impact model of TiC particle-reinforced aluminum-matrix composite coating–pure aluminum alloy were constructed based on molecular dynamics simulation. The ablation resistance of the material was evaluated by analyzing the depth of arc impact, the mass loss of the model, the number of gasification atoms, and the surface temperature of the material. The protection mechanism of the modified layer on the substrate was revealed by analyzing the damage degree of the surface and subsurface of the material after arc impact. The results showed that the strengthening mechanism of TiC particle-reinforced aluminum-matrix composites included fine grain strengthening, dispersion strengthening, dislocation strengthening, and so on. Covering TiC particle-reinforced aluminum-matrix composite coating on the surface of aluminum alloy armature is helpful in improving its ablation resistance. The research results can provide a theoretical basis and technical support for the modification design and performance control of electromagnetic rail armature.



Citation: Fan, C.; Zhang, L.; Kurbonov, N.N.; Rakhmonov, I.U.; Wang, G. Research on the Ablation Resistance of TiC Particle-Reinforced Aluminium-Based Composite Coatings on Armature Surface. *Coatings* **2024**, *14*, 549. <https://doi.org/10.3390/coatings14050549>

Academic Editor: Philipp Vladimirovich Kiryukhantsev-Korneev

Received: 11 April 2024

Revised: 25 April 2024

Accepted: 26 April 2024

Published: 28 April 2024



Copyright: © 2024 by the authors. Licensee MDPI, Basel, Switzerland. This article is an open access article distributed under the terms and conditions of the Creative Commons Attribution (CC BY) license (<https://creativecommons.org/licenses/by/4.0/>).

1. Introduction

Electromagnetic rail launch technology is a kind of launch technology that uses armature to accelerate a load to ultra-high speed in milliseconds, driven by the Lorentz force in a strong magnetic field. It has outstanding advantages such as high controllability, fast response, and high kinetic energy [1]. It can solve many unfavorable factors such as low launch efficiency, low energy levels, and poor control performance shared by traditional mechanical and chemical energy launches. It can be applied to rocket and satellite launches, aircraft launches, and high-speed electromagnetic train driving, and it has very broad application prospects.

The working conditions of electromagnetic rail launch systems show characteristics of extreme complexity. The pulse high current is MA-level, the working time is ms-level, the contact pressure of the armature rail is 100 Mpa-level, and the relative speed of the armature rail can reach 2.5 km/s. On the one hand, under the impact of pulsed high current, the transition phenomenon easily occurs between the armature and rail, and the sliding arc in the chamber causes a stronger energy arc, which causes serious ablation of the armature metal material; on the other hand, the heat generated by the arc vaporizes the

surface of the armature instantaneously, and a large amount of aluminum vapor causes a more intense arc discharge, resulting in melting splashing and evaporation erosion of the material, which seriously restricts the long-term service stability of the electromagnetic energy equipment under extreme conditions [2]. This puts forward higher requirements for the ablation resistance of the armature material [3]. Therefore, it is of great significance and engineering value to study the surface modification methods of armature materials in extremely complex environments to improve the reliability of electromagnetic rail launch and accelerate its engineering application.

Addressing the problem of the damage suppression of armature and rail materials, Bolin Cai [4] proposed that armature erosion can be suppressed by highly temperature-resistant, highly conductive thermal materials without affecting launch efficiency. At present, various kinds of carbon materials, metals, and ceramics are widely used as surface modification reinforcements [5].

At present, graphene-reinforced polymers are widely used as a means of increasing the strength of a material while maintaining its plasticity [6,7]. Numerous studies have reported that the mechanical, thermal, and electrical properties of materials can be improved by adding graphene nanoparticles to the aluminum matrix [8–10]. However, graphene has a small volume but a large specific surface area, which means that it easily agglomerates in the process of ball milling and mixing, resulting in poor bonding between the graphene and the metal matrix. Additionally, graphene is highly susceptible to oxidation at high temperatures in an aerobic environment, so it is not suitable as a surface modification material for electromagnetic gun aluminum alloy armature. Junwei Ye and other researchers [11–13] first proposed the concept of high-entropy alloys. According to the characteristics and functions of each metal element, a high-entropy alloy coating with “cocktail” performance is formed according to different ratios, which can greatly improve the surface performance of the armature material. Hsu [14] prepared NiCo_{0.6}Fe_{0.2}Cr_{1.5}SiAlTi_{0.2} HEA coatings with plasma cladding equipment and found that a large amount of Cr₃Si phase was formed in the coating, and the hardness and wear resistance were greatly increased when aging at 800 °C and 1100 °C. Cai [15] prepared NiCrCoTiVAl alloys on a Ti-6Al-4V substrate through laser cladding, and the phase structure remained unchanged after being held at 900 °C for 8 h. The results showed that the coating was stable below 1005 °C. However, the composition design of high-entropy alloy coatings lacks systematic theoretical support, and the relationship between elements and alloys is still unclear. Most of them consist of “cocktail-style” blending [16], and high-entropy alloys are multi-principal element alloys. This paper is devoted to the study of single-principal element reinforced composites with aluminum as the main element.

The American Standard Test Method (ASTM) defines cermets as heterogeneous materials composed of one metal or alloy with one or more ceramics, in which the volume of metal accounts for 15%–85% [17,18]. The metal–ceramic composite material has the comprehensive advantages of both metal and ceramic. The ceramic material has high hardness, strong wear resistance, and good thermal conductivity. However, due to its brittleness, it is not easy to process due to its sensitivity to stress and cracks. The preparation of metal–ceramic composite coatings can solve the above problems to a certain extent [19]. Currently, ceramic particle-reinforced aluminium-matrix composites are prepared by a powder metallurgy and in-situ autogenous method, in which the manufacturing process of the powder metallurgy method is relatively complex and costly, and, after adding a large number of ceramic particles, the plasticity of the material is significantly reduced, which leads to poor formability in secondary processing. The in-situ synthesis method has the advantages of small particle size, regular shape, high stiffness, and clean interface [20–22], and has become an important preparation method for high-performance particle-reinforced aluminum-matrix composites. The in-situ synthesized reinforced particles in aluminum-matrix composites mainly include TiB₂, TiC, Al₂O₃, ZrB₂, TiN, and TiAl₃ [23–27]. Among them, TiC particles have advantages such as a high melting point and high hardness, which are widely chosen as a hard ceramic reinforcement. Pradeep [28] prepared Al-10 wt% TiC

and Al-5 wt% TiC composites by in-situ synthesis. Zhang [29], Jiang [30], Zhuang [31], and Wang [32] formed TiC aluminum-matrix composites for an Al-Cu alloy, 5052 aluminum alloy, 6061 aluminum alloy, and 7075 aluminum alloy, respectively. Studies have shown that a small amount of in-situ TiC can improve the tensile strength, hardness, and ablation resistance of the composites. When the content of in-situ TiC is high, a large number of agglomerates will be formed at the grain boundary, reducing the bonding strength between the matrix and the reinforcement, and the strength and plasticity decrease simultaneously but the high hardness agglomerates cause the overall hardness of the composite to increase linearly. In this study, without changing the existing structure and main materials of the armature, only the arc root motion and residence area of the armature surface were modified and designed. Therefore, the TiC particle-reinforced aluminum-matrix composite coating was prepared on the surface of the armature, which was expected to improve the ablation resistance of the armature.

Based on molecular dynamics simulation, this study constructed a pure aluminum alloy model and TiC particle-reinforced aluminum-matrix composite coating–pure aluminum alloy composite model. Then, the arc impact simulation of each model was carried out. The anti-ablation performance of the material was analyzed by the depth of arc bombardment, the number of evaporated atoms, and the mass loss of the model. The evolution of the microstructure of the material was revealed by the degree of atomic shear strain and DXA analysis to study the anti-ablation mechanism of TiC particle-reinforced aluminum-matrix composites.

2. Arc Impact Model Construction and Simulation Condition Settings

2.1. Arc Impact Model Construction

In the process of electromagnetic launch, physical processes such as magnetism, heat, and force are coupled with each other. Under the combined action of friction heat, joule heat, and arc heat, the armature and rail will melt, splash, and even evaporate, and the formed metal vapor enters the gap between the armature and rail and transforms into a plasma state, which leads to the transition of the armature rail gun from good sliding electrical contact to destructive arc contact [33], thus causing more serious erosion to the metal material of the armature and rail.

In this study, LAMMPS [34] (Large-scale Atomic/Molecular Massively Parallel Simulator) was used to simulate the arc impact process of the pure aluminum alloy model and TiC particle-reinforced aluminum-matrix composite coating–pure aluminum alloy composite model. The simulation setting of the arc impact damage model was as follows:

- (1) The arc was essentially a beam of the free gas discharge phenomenon. The melting point of TiC was above 3200 K, and its properties were extremely stable. However, the melting and boiling point of the aluminum alloy was low, and it was easier to vaporize than TiC ceramic particles at high temperatures. Therefore, the arc was equivalent to a bunch of high-speed and high-temperature aluminum atoms in this model.
- (2) The in-situ generated TiC particles were dispersed in the aluminum alloy matrix, and the distribution was relatively uniform when the mass fraction was small, and there was basically no agglomeration phenomenon [32]. TiC is a gray, metal-like, face-centered, cubic lattice solid, so it was assumed that TiC particles were uniformly dispersed in the aluminum alloy matrix in a regular tetragonal form.
- (3) The material of the actual armature was 6063 aluminum alloy and the shape was ‘C’. There was an enhanced modification design of the arc root motion and residence area of the armature surface, and the Al element content in the 6063 aluminum alloy accounted for more than 97.5%, so this part of the armature was simplified to a tetragonal shape, and the aluminum alloy armature was simplified to a pure aluminum armature.

The model establishment process was as follows: First, the CIF file of TiC was downloaded from the Materials Project website to obtain its atomic structure information. A square aluminum matrix with a side length of 20 Å was constructed, and a square with

a side length of 6 Å was hollowed out from its center and filled with TiC particles to obtain a TiC particle-reinforced aluminum-matrix composite unit. The unit was expanded by $5 \times 5 \times 4$ cells to obtain a TiC particle-reinforced aluminum-matrix composite model of $100 \text{ \AA} \times 100 \text{ \AA} \times 80 \text{ \AA}$. The below atoms of the model were removed and filled with aluminum atoms, and only the modified layer with a thickness of 15 Å was retained to establish a TiC particle-reinforced aluminum-matrix composite coating–pure aluminum alloy composite model. Finally, the cylindrical region was randomly filled with aluminum atoms to 60 Å above it to form an arc impact model. The model establishment process is shown in Figure 1. In order to observe the distribution of TiC particles in the aluminum matrix, the aluminum matrix is transparentized.

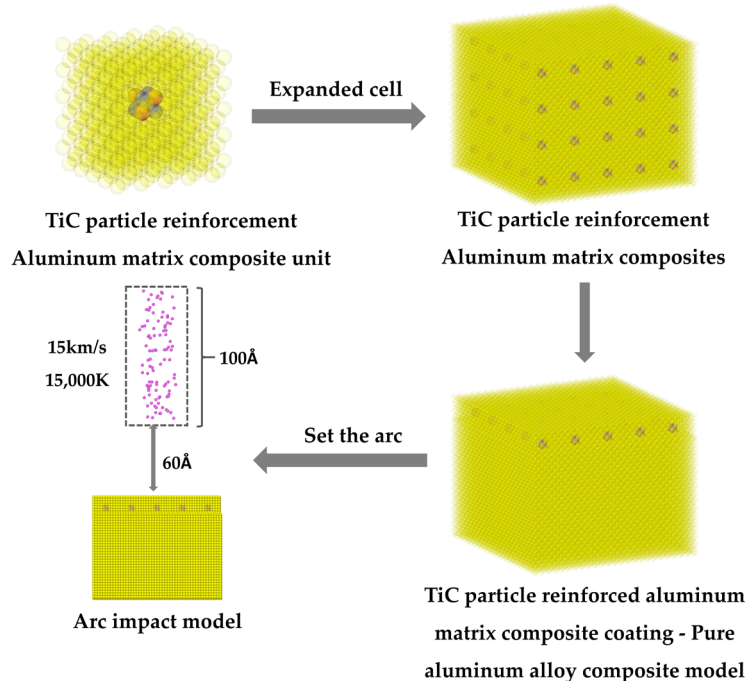


Figure 1. Arc impact model establishment process.

2.2. Simulation Parameter Settings

2.2.1. Potential Function Setting

In molecular dynamics calculations, the potential function describes the interaction between particles in the system, which can directly affect the accuracy and efficiency of the simulation system.

The EAM potential function [35] is used to calculate the pairwise interaction between the metal and metal alloy. The calculation formula for the total energy of the atom is below:

$$E_{\text{tot}} = \frac{1}{2} \sum_{ij} \varphi_{ij}(r_{ij}) + \sum_i F_i(\bar{\rho}_i) \quad (1)$$

where $\varphi_{ij}(r_{ij})$ is the pair potential interaction of atom i and j at distance r_{ij} , F_i is the embedding energy of atom i, and $\bar{\rho}_i$ is the function of atomic electron density.

The alloy EAM potential function fitting procedure developed by Zhou can achieve the formation of alloy potential and normalized element potential of up to 16 metals including Al and Ti [36,37]. In this study, this potential was selected to describe the interaction between Al-Al and Al-Ti.

The 2NN MEAM potential function [38] was used between Ti and C, and the total energy $E_{\text{Ti-C}}$ was as follows:

$$E_{\text{Ti-C}} = \sum_i [F_i(\bar{\rho}_i) + \frac{1}{2} \sum_{i \neq j} \varphi_{ij}(r_{ij}) S_{ij}] \quad (2)$$

In the formula, S_{ij} is the screening function.

In 2NN MEAM, there are 14 potential parameters of pure components, which are cohesive energy E_c , equilibrium distance r_e , bulk modulus B , and parameters related to model and structure C_{\min} , C_{\max} , d , A , $\beta^{(0)}$, $\beta^{(1)}$, $\beta^{(2)}$, $\beta^{(3)}$, $t^{(1)}$, $t^{(2)}$, and $t^{(3)}$. Among them, E_c , r_e , and B can be obtained from experiments, and model and structure-related parameters can be obtained by fitting the static properties of the material. In addition to the above 14 parameters, the 2NN MEAM parameters of the binary system also require 12 potential parameters between the two components: E_c , r_e , B , $C_{\min}(XYX)$, $C_{\min}(XYY)$, $C_{\min}(YXY)$, $C_{\min}(XXY)$, $C_{\max}(XYX)$, $C_{\max}(YXY)$, $C_{\max}(XXY)$, $C_{\max}(XYY)$, and ρ_0^Y/ρ_0^X , where X is the left element and Y is the right element. The parameter values are shown in Tables 1 and 2.

Table 1. The 2NN MEAM potential parameters of Ti and C.

	E_c	r_e	B	A	$\beta^{(0)}$	$\beta^{(1)}$	$\beta^{(2)}$	$\beta^{(3)}$	$t^{(1)}$	$t^{(2)}$	$t^{(3)}$	C_{\min}	C_{\max}	d
Ti	4.87	2.92	1.10	0.66	2.70	1.00	3.00	1.00	6.80	-2.0	-12	1.00	1.44	0.00
C	7.37	1.54	4.44	1.18	4.25	2.80	2.00	5.00	3.20	1.44	-4.4	1.41	2.80	0.00

Table 2. The 2NN MEAM potential parameters between Ti-C bi-components.

	E_c	r_e	B	$C_{\min}(XYX)$	$C_{\min}(YXY)$	$C_{\min}(XXY)$	$C_{\min}(XYY)$	$C_{\max}(XYX)$	$C_{\max}(YXY)$	$C_{\max}(XXY)$	$C_{\max}(XYY)$	ρ_0^Y/ρ_0^X
Ti/C	6.90	2.21	241	0.64	1.19	0.64	1.19	2.70	2.80	1.44	2.80	6

The potential function at the Al-C interface used the Morse potential [39], with a total energy as follows:

$$E_{\text{Al-C}} = D_0 [e^{-2\alpha(r-r_0)} - 2e^{-\alpha(r-r_0)}] \quad r < r_c \quad (3)$$

In the formula, D_0 is the well depth of Morse potential, α is the related parameter of well depth and width, r is the distance between nuclei, r_0 is the equilibrium spacing, and r_c is the truncation radius.

The Morse potential parameters between Al-C interfaces are shown in Table 3.

Table 3. The Morse potential parameters between Al-C interfaces.

Parameter	D_0/eV	$\alpha/\text{\AA}^{-1}$	$r_e/\text{\AA}$
Value	0.4691	1.7328	2.246

2.2.2. Simulation Conditions Settings

In order to avoid the relaxation error caused by the excessive overlap of the initial model, after establishing the TiC particle-reinforced aluminum-matrix composite coating-pure aluminum alloy composite model, structure optimization was first carried out to remove the overlapping atoms in the modeling process, and the conjugate gradient method was set up to optimize the static structure. Then, with 1 fs as the time step, under the NVT ensemble, the temperature was set to 300 K for dynamic relaxation until the density, potential energy, temperature, pressure, and other parameters of the system did not change significantly with time, that is, the system had reached the state of relaxation equilibrium.

The structure was converted into a data file as the initial file for subsequent arc impact simulation. There were 49,850 atoms in the composite system. The length of the three sides of the aluminum matrix was $100 \text{ \AA} \times 100 \text{ \AA} \times 65 \text{ \AA}$. The thickness of the composite coating was 15 \AA and the volume fraction of TiC in the coating was 3.6%.

The model was set up with periodic boundary conditions in the x and y directions and contraction boundary conditions in the z direction. In order to keep the model stable during the arc impact process, it was grouped as shown in Figure 2. The model was composed of a fixed layer, thermostatic layer, Newton layer, and arc layer. The fixed layer was equivalent to an immovable rigid body that could prevent the structure from moving when the arc impacted. In order to reduce the calculation cost, the fixed layer atoms were not considered in the simulation process. The thermostatic layer was convenient for the heat conduction of the structure during the impact process, preventing the atomic velocity from increasing sharply and flying out of the simulation system. During the simulation process, the model was always maintained at 300 K under the NVT ensemble. The Newton layer was the area of arc impact and the arc layer was the area where high-temperature and high-speed aluminum atoms were randomly distributed. Both areas were set as NVE ensembles to ensure that the system energy did not change. The fixed layer size of the composite model was $100 \text{ \AA} \times 100 \text{ \AA} \times 5 \text{ \AA}$, the thermostatic layer size was $100 \text{ \AA} \times 100 \text{ \AA} \times 15 \text{ \AA}$, the Newton layer size was $100 \text{ \AA} \times 100 \text{ \AA} \times 65 \text{ \AA}$, and the arc layer was a cylindrical area with a radius of 15 \AA and a height of 100 \AA at 60 \AA above the model. Then, 100 aluminum atoms were randomly added to bombard the composite model along the z-axis negative direction at a speed of 15 km/s. After the arc impact, the whole model was cooled to a room temperature of 300 K under the NVT ensemble to achieve a stable state.

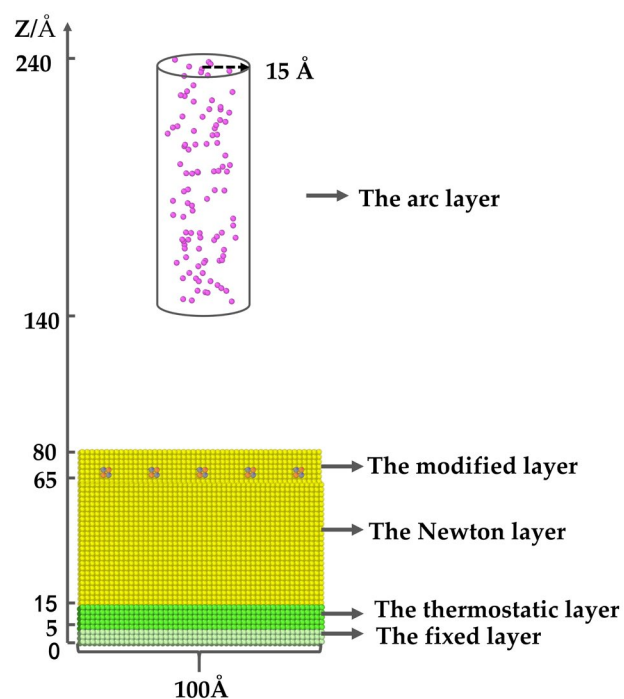


Figure 2. Simulation area division.

3. Results and Discussion

Under high-temperature and high-speed arc impact, the material undergoes melting, gasification, splashing, and other ablation processes. In order to evaluate the ablation protection effect of the TiC particle-reinforced coating on the matrix material, the depth of arc erosion, the mass loss during the ablation process, and the number of gasification atoms were used as the microscopic characterization of the ablation degree. The damage degree of the surface and subsurface of the material and the surface temperature of the material

after arc impact were analyzed to explore the effect of TiC particle doping on the ablation resistance of aluminum alloy from the micro-molecular level and reveal the anti-ablation mechanism of TiC particle-reinforced aluminum-matrix composites.

3.1. Arc Erosion Depth Analysis

The impact and erosion of the arc lead to changes in the surface morphology and composition of the material [40]. During the arc burning period, the temperature of the material rises sharply, and, when it rises to the melting point, a flowing molten pool is generated, and even splashing occurs; when it rises to the boiling point, the molten pool evaporates into metal vapor, resulting in evaporation loss. After the arc is extinguished, the gas and liquid materials condense into solids, accompanied by material transfer. The depth of arc erosion can reflect the micro-deterioration of the material during the dynamic process of arc erosion. After the arc impact, the distance between the deepest invaded aluminum atom and the upper surface of the material is regarded as the maximum erosion depth of the arc. The average distance between all the invaded aluminum atoms and the upper surface of the material is the average erosion depth of the arc, as shown in Table 4. By comparing the above two parameters, the arc impact ablation resistance of the pure Al and TiC/Al-Al systems was evaluated.

Table 4. The arc erosion depth of Al and TiC/Al-Al systems.

System	Maximum Arc Erosion Depth/Å	Average Arc Erosion Depth/Å
Al	22.34	5.66
TiC/Al-Al	12.70	2.23

Table 4 shows that the maximum arc erosion depth of the TiC/Al-Al system was about 43% lower than that of the pure Al system, and the average arc erosion depth was about 61% lower than that of the pure Al system. This shows that the TiC particle-reinforced aluminum-matrix composite coating helped to reduce the penetration depth of the arc in the armature, thereby improving the ablation resistance of the armature. The reasons for this are mainly divided into the following three points: First, because TiC and Al have the same crystal structure and similar lattice constants, the mismatch between atoms was within a reasonable range and the wettability with the matrix was good. This allowed TiC particles to be dispersed in the matrix in a more homogeneous form, with the effect of diffuse strengthening. Second, the melting point of TiC is high. When the temperature rise caused by arc impact was higher than the melting point of Al, TiC could still exist in the form of particles. During solidification, it was promoted by Al dendrites and enriched at grain boundaries, promoting the heterogeneous nucleation of crystals, inhibiting grain growth, effectively refining grains, and improving material strength. Thirdly, because the hardness of TiC particles is much higher than that of the Al matrix, when the material was impacted by the arc, the load was transferred from the metal matrix to the ceramic particle reinforcement, and the tensile strength of the material was enhanced.

Figure 3 shows the structural changes of the pure Al and TiC/Al-Al systems after arc shock. It can be seen that after the material was subjected to arc bombardment, the surface atoms splashed and the internal atoms deformed, deviating from the normal arrangement of the crystal structure. Compared with the pure Al system, the deformation atom range of the TiC/Al-Al system was smaller, and most of the bombarded aluminum atoms were blocked above the TiC particle doping area.

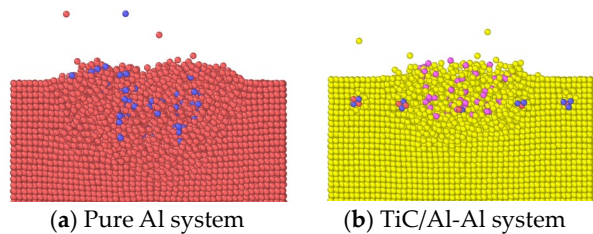


Figure 3. Model bombardment crater section.

In order to analyze the microstructural changes caused by the arc impact more intuitively, the atomic shear strain cloud diagram of the pure Al and TiC/Al-Al systems after arc bombardment and after cooling to room temperature was calculated by OVITO, and only the atoms with strain greater than 0.1 \AA in the model were retained. From Figure 4, it can be seen that after the arc impact, compared with the pure Al system, the strain atomic range of the TiC/Al-Al system was smaller and the strain degree was lower. It can be seen from Figure 5 that after the system was cooled to room temperature, the strain range of both systems was expanded. This is because the arc impact process generated energy transfer. The arc carrying high energy first transferred energy to the atoms on the surface of the material and then the energy continued to be transmitted downward in the form of a shock wave, causing the atoms inside the material to strain. Compared with the pure Al system, the deformation atom range of the TiC/Al-Al system was significantly reduced, and the strain degree was significantly reduced. The atomic shear strain cloud diagram of the pure Al system was nearly tetragonal, indicating that the shock wave propagated more evenly downward in the system until it decayed to 0. The strain cloud diagram of the TiC/Al-Al system was inverted conical because the addition of TiC particles made the matrix grains finer, and the fine grain reinforcement resulted in a more dispersed and faster decay of impact stresses in the coated armature. This is because the TiC particles were closely combined with the matrix. The additional load was transferred from the metal matrix to the reinforcement particles through the interface between the matrix and the reinforcement so that the matrix and the particle reinforcement bore the additional load together, thus resisting the deformation caused by the impact stress.

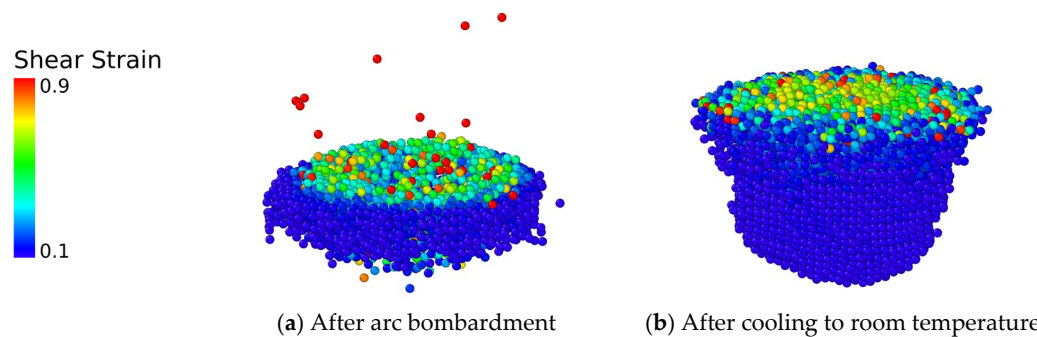


Figure 4. Atomic shear strain cloud diagram of pure Al system.

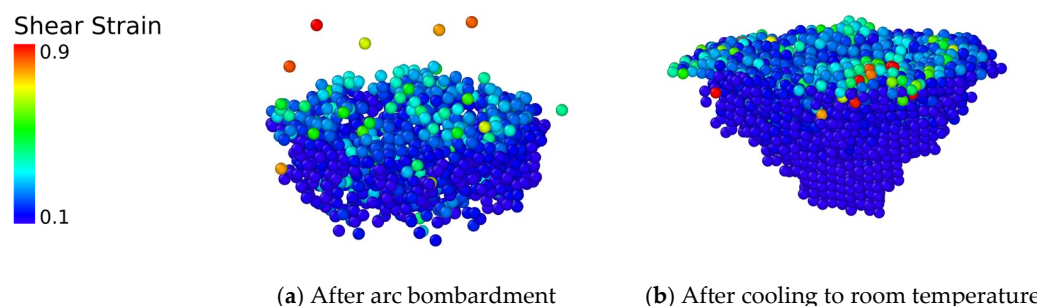


Figure 5. Atomic shear strain cloud diagram of TiC/Al-Al system.

3.2. Analysis of Material Mass Loss and the Number of Gasification Atoms

The electromagnetic rail launch process is accompanied by the generation and development of the arc. Under the action of ultra-high arc heat, the aluminum alloy armature rapidly melts or even vaporizes, and a large amount of aluminum vapor causes more intense arc discharge. In this study, the armature material was enhanced and modified to reduce the steam content of the aluminum alloy material due to ablation, thereby inhibiting the development of the arc. Therefore, it was necessary to analyze the degree of gasification and mass loss of the material under arc ablation. In order to quantify the ablation reduction effect of the TiC particle-reinforced aluminum alloy coating on the matrix, the normalized mass of the pure Al system and TiC/Al-Al system was calculated as shown in Figure 6. The normalized mass is the ratio of the remaining material mass to the initial mass of the material after the arc bombardment is completed and the system is stable.

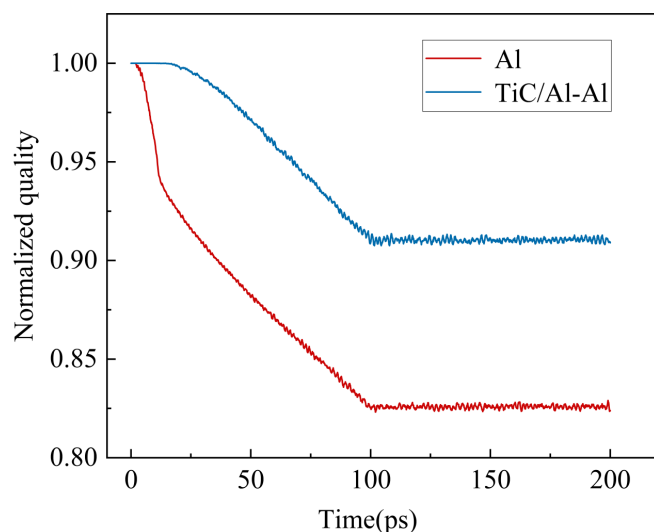


Figure 6. The normalized mass of pure Al system and TiC/Al-Al system.

The mass loss trends of the two systems were similar, and both decreased first and then reached dynamic equilibrium. The mass loss rate of the uncoated aluminum matrix after ablation was about 18% and the mass loss rate of the TiC/Al-Al composite was about 9%, which was lower than that of the pure aluminum alloy armature, indicating that the addition of TiC particles to modify the material was helpful to enhance the ablation resistance of the armature. From a microscopic point of view, since the reinforcing phase TiC was distributed around the matrix grains and the structure of the TiC particles was stable, the melting point could reach more than 3200 °C. When the aluminum matrix expanded outward by heating, it was hindered by TiC, so the thermal stability of the composite was improved. During the ablation process, due to the low evaporation latent heat of the aluminum, the aluminum atoms first vaporized and were exuded from the ceramic composite material, which played the role of 'sweating cooling' and protected the ceramic skeleton. Figure 7 shows the morphology change of TiC particles in the composite during arc ablation, in which Al atoms are deleted. It can be seen that under the action of high temperature, the ceramic skeleton grains grew, the phenomenon of large grains annexing small grains occurred, and obvious roundness occurred, which was conducive to further improving the strength of the ceramic skeleton and increasing the ablation resistance. Therefore, during the ablation process, the ability of the composite skeleton to resist heat flow erosion gradually increased, thereby improving its ablation resistance.

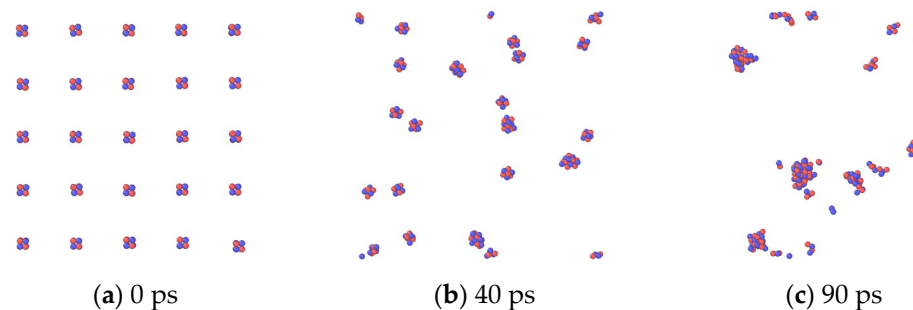


Figure 7. The morphology change diagram of TiC particles during arc ablation process.

A vacuum layer was set in the 110 Å–160 Å region above the material, and the variation of the number of atoms vaporized into the vacuum layer in the pure Al system and TiC/Al-Al system was counted, as shown in Figure 8. There was no atomic gasification of the pure Al system into the vacuum layer within 0–50 ps of arc ablation. This is because the temperature of the material had not reached the boiling point at the beginning of arc ablation, and the lowest vacuum layer was 30 Å away from the surface of the material. It takes a certain amount of time for gasification atoms to rise to a vacuum layer. In the TiC/Al-Al system, there were gasification atoms in the vacuum layer until 70 ps. With the progress of ablation, the number of atoms in the vacuum layer of the pure Al system increased rapidly and reached dynamic equilibrium at 120 ps. The number of atoms evaporating into the vacuum layer in the TiC/Al-Al system increased slowly and began to reach dynamic equilibrium at about 110 ps. This indicates that the use of TiC particle-reinforced aluminum-matrix composites to coat the aluminum alloy armature effectively reduced the amount of metal vapor generated, thereby reducing the arc energy and inhibiting its rapid growth. In addition, the change trend of the number of gasification atoms and the change trend of the normalized mass of the material could be mutually verified, which also verified the correctness of the model.

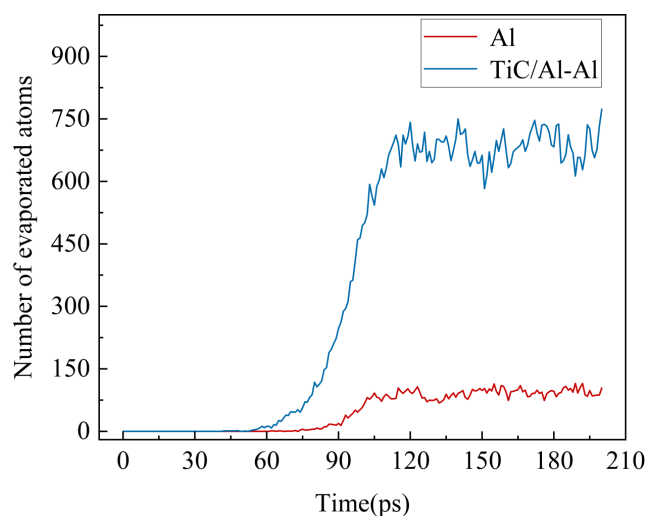


Figure 8. Changes in the total number of atoms in the vacuum layer of pure Al system and TiC/Al-Al system over time.

3.3. Material Surface Temperature Analysis

In the process of electromagnetic rail launch, the armature temperature will rise sharply, resulting in material melting and gasification, which is a very critical factor in the arc triggering mechanism. Therefore, it was necessary to analyze the change in material surface temperature caused by arc impact. The atoms in the matrix model from the top surface to the bottom 25 Å were set as the temperature measurement layer to study the temperature variation of the pure Al system and TiC/Al-Al system effected by the arc

impact. Figure 9 shows the variation in the temperature of the pyrometry layer of the two systems over time under a bombardment speed of 15 km/s. The peak temperature of the pyrometry layer of the TiC/Al-Al system was 2815 K, which was 22% higher than that of 2309 K of the pure Al system. Figure 10 is the X-Y two-dimensional temperature cloud diagram of the surface of the two types of materials at the end of the arc bombardment. Because the arc bombardment position set by this model was the material center, and the arc action time was extremely short, the heat had not yet been transmitted to a large number of surroundings, so the material center temperature was higher. The surface temperature of the TiC/Al-Al system was higher than that of the pure Al system, and the high temperature range was smaller than that of the pure Al system. It can be seen that the addition of TiC particles reduced the thermal conductivity of the aluminum alloy armature.

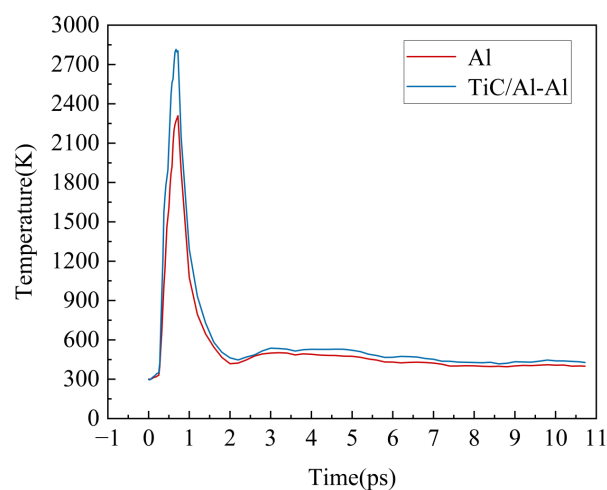


Figure 9. The temperature change of the temperature measurement layer of the two systems over time.

In the composites, the low thermal conductivity of TiC (21 W/m·K) and the material lattice distortion induced by the incorporation of ceramic particles reduced the thermal conductivity of the aluminum alloy armature. The lattice distortion of the aluminum alloy matrix caused by the ceramic particles reduced the thermal conductivity of the aluminum alloy matrix. The thermal conduction mechanism of metal mainly includes two parts [41]: electronic thermal conduction and lattice thermal conduction. First, hot electrons diffuse in the temperature field. As the temperature increases, free electrons accelerate and diffuse around, and cold electrons exchange energy through collision, thereby conducting heat. The second is lattice vibration. Lattice vibration is small at low temperatures, the number of phonons is small, and the average free path is long, so lattice thermal conductivity is strong. At high temperatures, the average free path of phonons will be significantly reduced and the thermal conductivity of the lattice will also be greatly reduced or even negligible. In addition, the increase in temperature also promotes the movement of free electrons, shortens the average free path, and weakens the ability of electrons to conduct heat. Therefore, the thermal conductivity of aluminum-matrix composites also decreases with increasing temperature. The solute atoms, precipitated phases, and lattice defects including dislocations, grain boundaries, and twins in the aluminum matrix will scatter free electrons to weaken its thermal conductivity. Therefore, the enhanced particle morphology and the dislocations and lattice distortions induced by ceramic particles will have a greater impact on the thermal conductivity of the matrix. However, compared with the huge scattering effect of solute atoms on free electrons in copper alloys, ceramic particles have little effect on thermal conductivity [42,43]. Therefore, the use of ceramic particles to enhance aluminum-matrix composites can improve the strength of the aluminum matrix while reducing the weakening of its thermal conductivity. It is a more effective strengthening

method. In addition, the reduction of the thermal conductivity of the composite coating can delay the transfer of arc heat to the substrate.

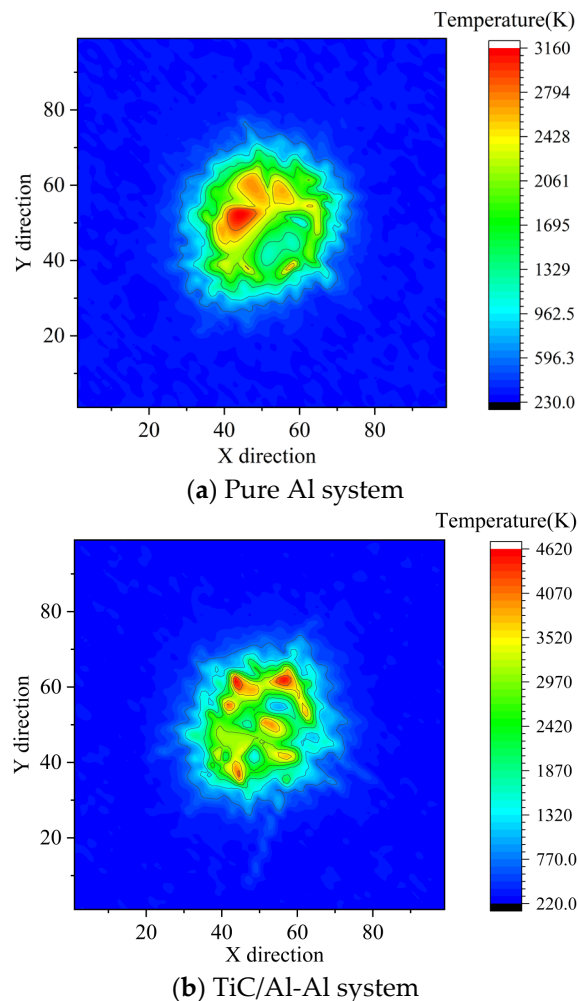


Figure 10. The temperature cloud diagram of the two systems at the end of arc bombardment.

3.4. Surface Morphology Analysis

The change in material surface morphology caused by arc impact can reflect the mechanical properties and ablation resistance of materials. Figures 11 and 12 show the change in the surface morphology of the pure Al system and TiC/Al-Al system over time under arc impact. Figures 11a and 12a are the surface morphology of the two systems at the end of the arc impact. It can be seen that under high-energy arc impact, the surface material of the substrate began to be heated, and the material beyond the melting point underwent phase transformation stripping and was gradually removed. Figures 11b–d and 12b–d show the change in the surface morphology of the pure Al system and TiC/Al-Al system in the time from the end of arc impact to cooling to room temperature. Firstly, the ablation pit expanded along the depth direction. This is because the material was subjected to arc impact for a short time, the energy density of the material center was high, and the heat transfer to the depth direction was more intense than the radial direction, so the material was eroded more obviously along the depth direction. As the heat transfer process continued, the area outside the center absorbed enough heat and began to melt and vaporize, and the pit expanded along the radial direction. Due to the temperature gradient in the radial heat transfer process, the molten material produced a surface tension gradient, and the partially molten material moved upward from the pit to the surface, that is, the Marangoni effect occurred, forming a bulge on the ablated surface and forming a recast

layer after cooling. Compared with the pure Al system, the surface morphology of the TiC/Al-Al system was more irregular, the impact crater was more flat, and the trend of radial development was more obvious. This is because TiC particle-reinforced aluminum-matrix composites have the effect of load transfer strengthening and micromechanical strengthening, which is beneficial for the improvement of material strength.

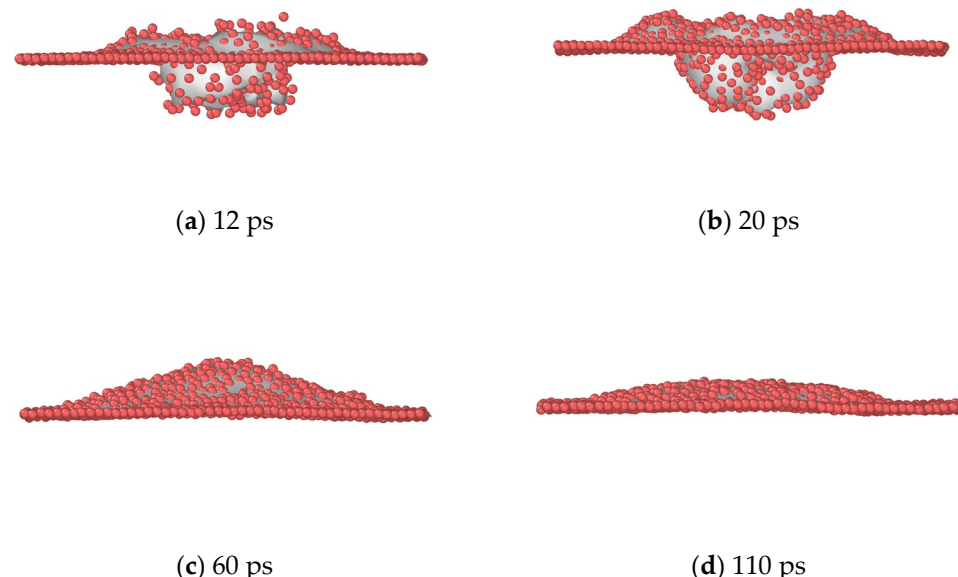


Figure 11. The surface morphology of pure Al system arc bombardment.

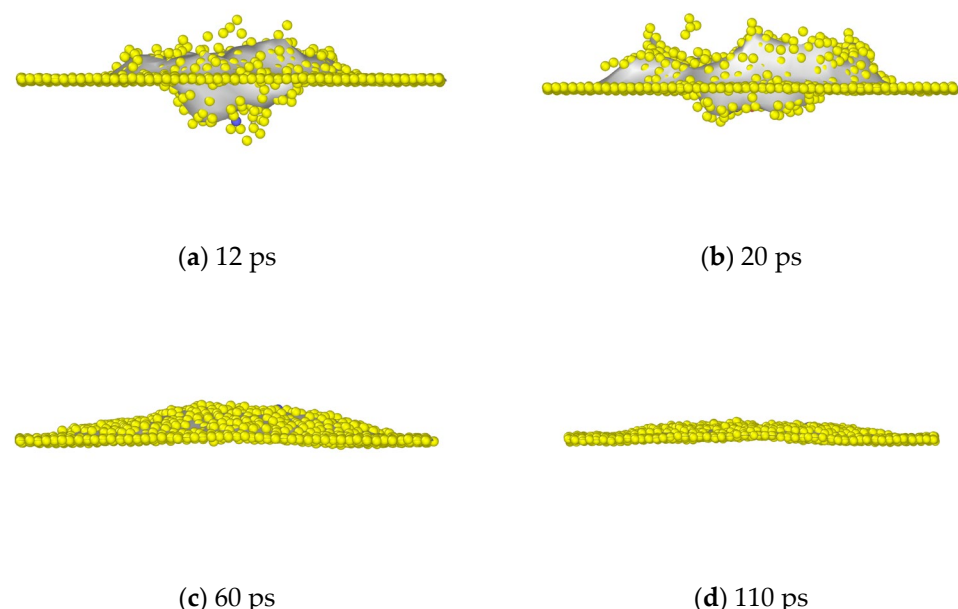


Figure 12. The surface morphology of TiC/Al-Al system arc bombardment.

To quantitatively characterize the surface damage degree of the material, the surface atomic coordinates of the material were extracted and the RMS deformation degree at each moment was calculated. The results are shown in Figure 13. At 20 ps, 40 ps, 60 ps, 80 ps, and 110 ps, the surface RMS deformation of the TiC/Al-Al system was 23%, 14%, 46%, 59%, and 49% smaller than that of the pure Al system, and the TiC/Al-Al system could reach a stable state faster after the impact. This is due to the fact that the hard TiC particles were dispersed in the composites and acted as pinning agents in the matrix, which increased the resistance to dislocation and grain boundary movement, resulting in the improved mechanical properties of the material.

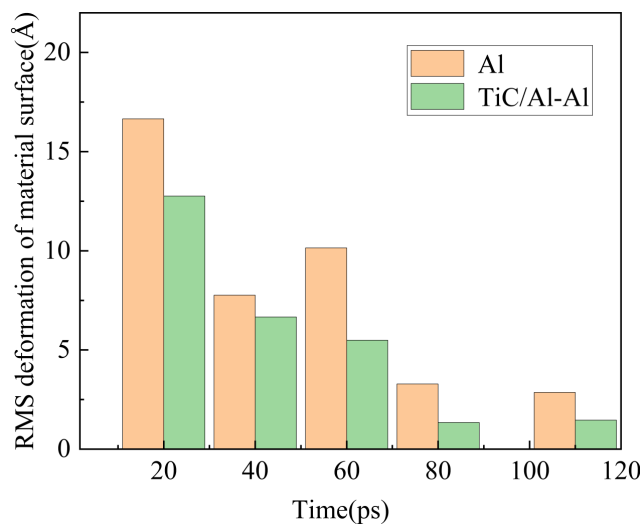


Figure 13. The RMS deformation of the material surface.

3.5. Subsurface Damage Analysis

Arc impact will not only cause damage to the surface of a material but also subsurface damage below the surface. Subsurface damage not only affects the integrity of the function of the material itself but may also eventually lead to the failure of the material, and its degree of damage can be expressed by the dislocation density in statistical molecular dynamics simulation. The ratio of the total length of the dislocation line to the volume of the material is the dislocation density, and, since the volume size of the model was constant in this study, the trend of the dislocation length was consistent with the trend of the dislocation density. The Dislocation Extraction Analysis (DXA) module in OVITO 3.7.9 software was used to calculate and output the dislocation length in combination with its internal Python interface, as shown in Figure 14.

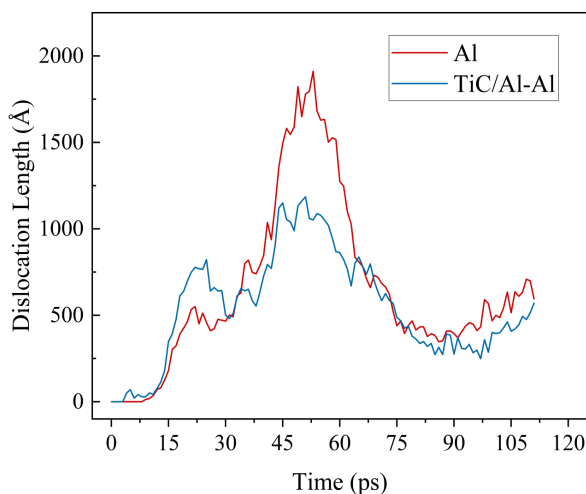


Figure 14. The total dislocation line length of the two systems.

Figure 14 shows the length of the total dislocation line in the two systems. It can be seen from the figure that there were almost no dislocations in the two systems before the arc impact. After the arc impact, due to the existence of the second-phase hard particle in the TiC/Al-Al system, the dislocation pinning effect brought by it caused the dislocation to be unable to cut through and only able to bypass, so the total length of the dislocation line in the system increased greatly. In the process of the system gradually returning to stability, the dislocation line length of the pure Al system was larger. This is because the TiC-reinforced aluminum-matrix composite coating had a certain protective effect on the

Al matrix, which made the damage to the TiC/Al-Al system lesser. In order to analyze the reason, the dislocation evolution process inside the two systems was extracted, as shown in Figures 15 and 16. In the figures, OTHER- and FCC-type atoms are deleted, and only dislocation and HCP-type atoms are retained.

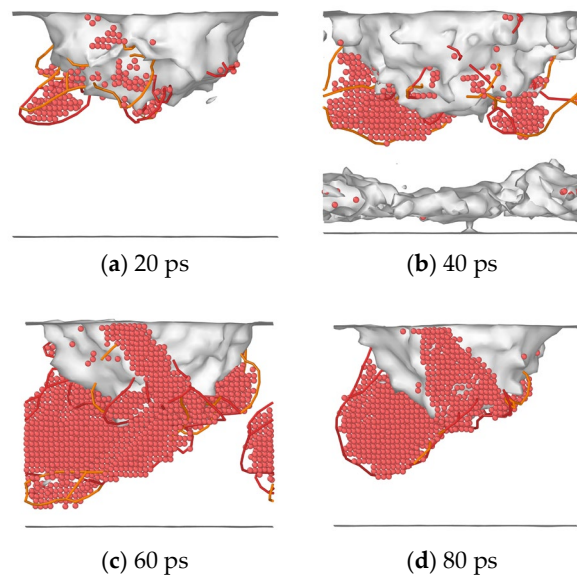


Figure 15. The dislocation evolution process in pure Al system.

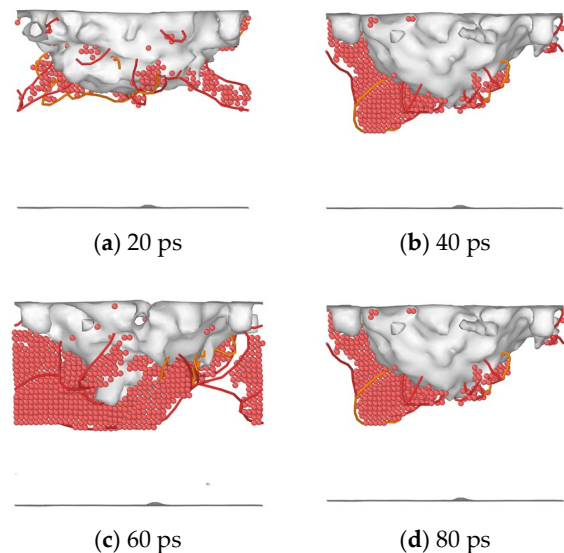


Figure 16. The dislocation evolution process in TiC/Al-Al system.

It can be observed that at 20 ps, the pits in the TiC/Al-Al system had a clear trend of radial development, while the pits in the pure Al system extended more obviously in the longitudinal direction. This phenomenon was more intuitive at 60 ps. The dislocation line and HCP-type atoms in the pure Al system almost touched the bottom of the material. While, in the TiC/Al composite system, the defects of the material caused by arc impact ablation were lighter, and it was due to the dislocation pinning effect of the TiC particles. At 80 ps, the pure Al system had not yet reached a stable state, and there were many defects at the bottom of the material, while the TiC/Al composite system had almost reached a stable state. The reason is that under the action of arc impact, small holes were generated at the material interface and cracks were transmitted and developed near the interface. There was a stress field near the interface due to lattice distortion. When the dislocation passed

through, it was necessary to perform more work to tear the interface, so the yield strength of the TiC/Al composites was significantly upgraded.

3.6. Total Consequence and Discussion

In this section, the simulation process of arc impact is analyzed and the strengthening mechanism of the TiC particles in the aluminum matrix is explored. The simulation results show that compared with the pure Al system, the arc erosion depth of the TiC/Al-Al system was significantly reduced, the degree of internal atomic strain was reduced, and the material mass loss caused by the impact ablation of the arc was also reduced. In addition, the surface and subsurface damage of the armature coated with the modified layer was lower than that of the pure Al alloy armature. Combining the simulation results with theoretical analysis, the following conclusions are drawn: the strengthening mechanism of TiC particle-reinforced aluminum-matrix composites includes fine grain strengthening, dispersion strengthening, and dislocation strengthening and covering TiC particle-reinforced aluminum-matrix composite coatings on the surface of the aluminum matrix is helpful to reduce the impact ablation effect of arc on the armature.

4. Conclusions

In this paper, the arc impact process of a pure aluminum alloy model and TiC particle-reinforced aluminum-matrix composite coating–pure aluminum alloy composite model was carried out through molecular dynamics simulation. The effect of TiC particle doping on the ablation resistance of the aluminum alloy was studied at the micro level, and the ablation resistance mechanism of TiC particle-reinforced aluminum-matrix composites was revealed.

- (1) TiC particles have fine grain strengthening, dispersion strengthening, and other strengthening effects on the aluminum matrix, which improves the strength of the composite. The ultra-high melting and boiling points of TiC particles give the TiC particle-reinforced aluminum-matrix composite coatings good thermal stability. This reduces the loss of material mass under the impact of high-energy, high-heat arc and results in the improved ablation resistance of the aluminum alloy armature.
- (2) The thermal conductivity of TiC particles is low and the lattice distortion caused by its incorporation reduces the thermal conductivity of the composite. This leads to an increase in the temperature of the material surface, which accelerates the phase transformation of the material. However, the effect of ceramic particles on thermal conductivity is smaller, and the improvement of material ablation resistance it brings is more considerable.
- (3) The tensile and yield strengths of TiC particle-reinforced aluminum-matrix composites are improved, which helps to reduce the surface and subsurface damage caused by arc impact on the matrix, indicating that the addition of TiC particles improves the impact resistance of the material.

Author Contributions: Conceptualization, C.F.; Methodology, C.F.; Validation, N.N.K.; Resources, L.Z., N.N.K., I.U.R. and G.W.; Data curation, C.F.; Writing—original draft, C.F.; Writing—review & editing, L.Z.; Supervision, L.Z. and I.U.R. All authors have read and agreed to the published version of the manuscript.

Funding: This work was supported by the National Natural Science Foundation of China, project 92166110.

Institutional Review Board Statement: Not applicable.

Informed Consent Statement: Not applicable.

Data Availability Statement: Data are contained within the article.

Conflicts of Interest: The authors declare no conflict of interest.

References

1. Jia, Q. Research on Electromagnetic Railgun Technology and Application. Master's Thesis, North Central University, Taiyuan, China, 2012.
2. Ma, W.M. Some thoughts on the development of cutting-edge technologies in electrical engineering disciplines. *J. Electrotechnol.* **2021**, *36*, 4627–4636. [[CrossRef](#)]
3. Chen, S.; Ma, Y.B.; Zhao, W.Y.; Tang, X.Y. Recent Research Progress and Application Prospects of Electromagnetic Rail Gun. *Sci. Technol. Innov. Appl.* **2022**, *12*, 11–14. [[CrossRef](#)]
4. Cai, B.L.; Feng, G. Current status of research on material damage suppression methods for electromagnetic orbital launchers. *Weapon Mater. Sci. Eng.* **2024**, *47*, 122–130. [[CrossRef](#)]
5. Tian, X.H.; Yang, X.D.; Liu, Y.; Wang, L. Current status of research on laser cladding coating materials. *Therm. Process.* **2024**, *53*, 1–5+9. [[CrossRef](#)]
6. Gao, Y.; Wu, Y.; Liu, J.; Zhang, L. Controlling the Electrical Conductive Network Formation of Polymer Nanocomposites via Polymer Functionalization. *Soft Matter* **2016**, *12*, 9738–9748. [[CrossRef](#)]
7. Shtein, M.; Nadin, R.; Buzaglo, M.; Kahil, K.; Regev, O. Thermally Conductive Graphene-Polymer Composites: Size, Percolation, and Synergy Effects. *Chem. Mater.* **2015**, *27*, 2100–2106. [[CrossRef](#)]
8. Wei, S.; Ke, Z.; Tian, W.; Rui, Z.; Yihao, W.U.; Bin, Z.; Ya, Y. Research Progress of Graphene Reinforced Aluminum Matrix Composites. *Nonferrous Mater. Eng.* **2019**.
9. Thiraviam, R.; Ravisankar, V.; Krishnan, P.K.; Arunachalam, R. Microstructural and Mechanical Properties of Alreinforced with Micro and Nano Al_2O_3 Particles Using Stir-Squeeze Casting Method. *Int. J. Mech. Prod. Eng. Res. Dev.* **2020**, *10*, 193–202. [[CrossRef](#)]
10. Zhang, L.; Hou, G.; Zhai, W.; Ai, Q.; Feng, J.; Zhang, L.; Si, P.; Ci, L. Aluminum/Graphene Composites with Enhanced Heat-Dissipation Properties by in-Situ Reduction of Graphene Oxide on Aluminum Particles. *J. Alloys Compd. Interdiscip. J. Mater. Sci. Solid State Chem. Phys.* **2018**, *748*, 854–860. [[CrossRef](#)]
11. Dou, W.; Chen, C.; Zhang, G.S.; Xu, L.J.; Mao, F.; Wei, S.Z. Current status of research on high-entropy alloy coatings. *Plat. Finish.* **2023**, *42*, 33–42. [[CrossRef](#)]
12. Liang, D.; Zhou, W.B.; Gong, X.L.; Song, X.L.; Xing, D.F.; Wang, H.C. The concept of high-entropy alloys and their characteristics. *China Met. Bull.* **2019**, *4*, 223–224.
13. Zhou, H.; Yang, S.F.; Yang, Y.N.; Yan, X.; Yang, W.; Tian, H.D. Research progress and development trend of high entropy alloys. *Therm. Process.* **2018**, *47*, 5–9. [[CrossRef](#)]
14. Hsu, W.L.; Yang, Y.C.; Chen, C.Y.; Yeh, J.W. Thermal Sprayed High-Entropy $\text{NiCo}_{0.6}\text{Fe}_{0.2}\text{Cr}_{1.5}\text{SiAlTi}_{0.2}$ Coating with Improved Mechanical Properties and Oxidation Resistance. *Intermetallics* **2017**, *89*, 105–110. [[CrossRef](#)]
15. Cai, Z.; Cui, X.; Jin, G.; Liu, Z.; Zheng, W.; Li, Y.; Wang, L. Microstructure and Thermal Stability of a Ni-Cr-Co-Ti-V-Al High-Entropy Alloy Coating by Laser Surface Alloying. *Met. Mater. Int.* **2017**, *23*, 1012–1018. [[CrossRef](#)]
16. Huang, Z.F.; Zhang, C.; Tang, Q.H.; Dai, P.Q.; Wu, B. Influence of annealing on the organisation and hardness of laser-melted FeCoCrNiB high-entropy alloy coatings. *Surf. Technol.* **2013**, *42*, 9–13. [[CrossRef](#)]
17. Ma, H.Y.; Pang, X.M.; Wang, J. Research on the preparation of selective absorption coatings on cermet by laser cladding. *Chem. Mach.* **2019**, *46*, 674–678+714.
18. Wang, X.R.; Li, H.; Yan, H.Y.; Liang, J.L. Progress in the application of metal-based ceramics. *Therm. Process.* **2019**, *48*, 12–15. [[CrossRef](#)]
19. Fan, P.F.; Sun, W.L.; Wang, K.D.; Zhang, G. Organisation and properties of laser clad metal-ceramic composite coatings on tooth wheel drill steels. *Therm. Process.* **2019**, *48*, 99–102. [[CrossRef](#)]
20. Vadayar, K.S.; Rani, S.D.; Prasad, V.V.B. Microstructural and Mechanical Characteristics of In-Situ Titanium Metal Matrix Composites. *Int. J. Theor. Appl. Res. Mech. Eng.* **2013**, *2*, 12–16.
21. Lakshmi, S.; Lu, L.; Gupta, M. In Situ Preparation of TiB₂ Reinforced Al Based Composites. *J. Mater. Process. Technol.* **1998**, *73*, 160–166. [[CrossRef](#)]
22. Ma, Y.; Addad, A.; Ji, G.; Zhang, M.X.; Ji, V. Atomic-Scale Investigation of the Interface Precipitation in a TiB₂ Nanoparticles Reinforced Al-Zn-Mg-Cu Matrix Composite. *Acta Mater.* **2020**, *185*, 287–299. [[CrossRef](#)]
23. Bian, Y.; Gao, T.; Liu, G.; Ma, X.; Ren, Y.; Liu, X. Design of an In-Situ Multi-Scale Particles Reinforced ($\text{Al}_2\text{O}_3+\text{ZrB}_2+\text{AlN}$)/Al Composite with High Strength, Elasticity Modulus and Thermal Stability. *Mater. Sci. Eng. A Struct. Mater. Prop. Misrostruct. Process.* **2020**, *775*, 138983. [[CrossRef](#)]
24. Yang, H.; Zhao, K.; Nie, J.; Liu, X. The Enhanced Superplasticity of a 2024 Matrix Nanocomposite Reinforced by TiC Particles. *Mater. Sci. Eng. A Struct. Mater. Prop. Misrostruct. Process.* **2020**, *774*, 138926. [[CrossRef](#)]
25. Emamy, M.; Mahta, M.; Rasizadeh, J. Formation of TiB₂ Particles during Dissolution of TiAl₃ in Al-TiB₂ Metal Matrix Composite Using an In Situ Technique. *Compos. Sci. Technol.* **2006**, *66*, 1063–1066. [[CrossRef](#)]
26. Duan, X.Z.; Xin, B.D.; Miao, T.J.; Xie, J.E.; Yang, H.Y.; Han, X.; Qiu, F.; Li, X.J. Microstructural and Performance Characterization of In-Situ Biphasic Micro-Nano Scale (TiB₂-TiC_x)/Al-Cu-Mg Composites with Different Ceramic and Metal Ratios Designed for Compact Integration. *J. Mater. Res. Technol.* **2020**, *9*, 3418–3429. [[CrossRef](#)]
27. Li, C.F.; Wang, J.; Li, K.; Shu, D.; Sun, B.D. Progress in the preparation of autogenous particle-reinforced metal matrix composites by in situ crystallisation. *Mater. Bull.* **2003**, *17*, 65–67.

28. Pradeep Kumar, G.S.; Koppad, P.G.; Keshavamurthy, R.; Alipour, M. Microstructure and Mechanical Behaviour of in Situ Fabricated AA6061–TiC Metal Matrix Composites. *Arch. Civ. Mech. Eng.* **2017**, *17*, 535–544. [[CrossRef](#)]
29. Zhang, D.S. Research on In-Situ Synthesis of TiC (TiB₂) Reinforced Al-Cu Alloy Matrix Composites by Microwave Heating. Master’s Thesis, Nanjing University of Science and Technology, Nanjing, China, 2020.
30. Jiang, S.Q.; Fan, Z.Y.; Zhou, Z.H.; Zhang, X.; Wang, Q.J. Organisation and mechanical properties of in situ synthesised TiC/5052 composites. *J. Ceram.* **2019**, *40*, 491–496. [[CrossRef](#)]
31. Khan, S.U. Study on the Preparation and Properties of In-Situ Synthesized TiC Particle Reinforced 6061 Matrix Composites. Master’s Thesis, Lanzhou University of Technology, Lanzhou, China, 2022.
32. Wang, R. Organisation and Properties of In Situ Autogenous TiC/7075 Composites. Master’s Thesis, China University of Mining and Technology, Beijing, China, 2016.
33. Tang, L.; He, J.; Chen, L.; Xia, S.; Feng, D.; Li, J.; Yan, P. Study of Some Influencing Factors of Armature Current Distribution at Current Ramp-Up Stage in Railgun. *IEEE Trans. Plasma Sci.* **2015**, *43*, 1585–1591. [[CrossRef](#)]
34. Plimpton, S. Fast parallel algorithms for short-range molecular dynamics. *J. Comput. Phys.* **1995**, *117*, 1–19. [[CrossRef](#)]
35. Zope, R.R.; Mishin, Y. Interatomic Potentials for Atomistic Simulations of the Ti-Al System. *Phys. Rev. B* **2003**, *68*, 366–369. [[CrossRef](#)]
36. Zhou, X.; Johnson, R.; Wadley, H. Misfit-Energy-Increasing Dislocations in Vapor-Deposited CoFe/NiFe Multilayers. *Phys. Rev. B* **2004**, *69*, 144113. [[CrossRef](#)]
37. Zhou, X.W.; Wadley, H.N.G.; Johnson, R.A. Atomic Scale Structure of Sputtered Metal Multilayers. *Acta Mater.* **2001**, *49*, 4005–4015. [[CrossRef](#)]
38. Kim, Y.M.; Lee, B.J. Modified Embedded-Atom Method Interatomic Potentials for the Ti–C and Ti–N Binary Systems. *Acta Mater.* **2008**, *56*, 3481–3489. [[CrossRef](#)]
39. Zhao, H.; Chen, N. An Inverse Adhesion Problem for Extracting Interfacial Pair Potentials for the Al (001)/3C–SiC (001) Interface. *Inverse Probl.* **2008**, *24*, 035019. [[CrossRef](#)]
40. Chun-Ping, W.U.; Jing-Chao, C.; Xiao-Long, Z. Silver Based Electric Contact Material. *Yunnan Metall.* **2005**.
41. Su, C.Y. Research on the Thermal Conductivity Mechanism of Magnesium Alloys Based on Solid Solution Atoms and Second Phase. Ph.D. Thesis, Shanghai Jiaotong University, Shanghai, China, 2020.
42. Miyake, J.; Ghosh, G.; Fine, M.E. Design of High-Strength, High-Conductivity Alloys. *Mrs Bull.* **1996**, *21*, 13–18. [[CrossRef](#)]
43. Li, Y.P.; Xiao, Z.; Li, Z.; Zhou, Z.Y.; Yang, Z.Q.; Lei, Q. Microstructure and Properties of a Novel Cu-Mg-Ca Alloy with High Strength and High Electrical Conductivity. *J. Alloys Compd. Interdiscip. J. Mater. Sci. Solid State Chem. Phys.* **2017**, *723*, 1162–1170. [[CrossRef](#)]

Disclaimer/Publisher’s Note: The statements, opinions and data contained in all publications are solely those of the individual author(s) and contributor(s) and not of MDPI and/or the editor(s). MDPI and/or the editor(s) disclaim responsibility for any injury to people or property resulting from any ideas, methods, instructions or products referred to in the content.